crystals

MDPI

Article

The Role of the Crystal Plane Irradiated by Swift Heavy Ions in the Formation of Defects in $MgAl_2O_4$ Crystals

Abdirash Akilbekov [1], Arseniy Kiryakov [2], Alexey Podshivalov [3], Zhulduz Ospanova [1], Gulnara Aralbayeva [1], Anatoli I. Popov [4,5], Zein Baimukhanov [1], Diana Junisbekova [1,*] and Alma Dauletbekova [1,5,*]

1 Institute of Physical and Technical Sciences, L.N. Gumilyov Eurasian National University, Satpayev Str. 2, Astana 010008, Kazakhstan; akilbekov_at@enu.kz (A.A.); zhulduz-ospan@mail.ru (Z.O.); agm_555@mail.ru (G.A.); zeinb77@mail.ru (Z.B.)
2 Institute of Solid State Chemistry of the Ural Branch of Russian Academy of Sciences, Pervomaiskaya Str. 91, Ekaterinburg 620990, Russia; arseny.kiriakov@urfu.ru
3 Institute of Physics and Technology of Ural Federal University, Mira Str. 19, Ekaterinburg 620002, Russia; a.p.podshivalov@urfu.ru
4 Institute of Solid-State Physics, University of Latvia, Kengaraga 8, LV-1063 Riga, Latvia; anatoli.popov@cfi.lu.lv
5 Latvian Academy of Sciences, Akademijas laukums 1, LV-1050 Riga, Latvia
* Correspondence: diana911115@gmail.com (D.J.); alma_dauletbek@mail.ru (A.D.)

Abstract

Model experiments were performed on the interaction of swift heavy 220 MeV Xe ions with $MgAl_2O_4$ spinel crystal with (100), (110), and (111) planes. A computational analysis of the energy parameters of Xe ions in $MgAl_2O_4$ single crystal was performed, and an estimate of the ion range in the near-surface layer (14 μm) was provided. Optical absorption spectrum was analyzed using polarized light and EPR spectroscopy of initial and irradiated crystals. It has been established that at a fluence of 10^{13} cm^{-2} in a sample with an orientation plane (110), 35% more optically active F-type centers are formed. It has been shown that optically active centers V_{Al}–O^- are observed in an unusual, polarized beam.

Keywords: $MgAl_2O_4$ single crystal; swift heavy ions; optical absorption spectra; electron paramagnetic resonance; F-type defects; V_{Al}–O^- centers

Academic Editor: Shin-ichi Kimura

Received: 5 October 2025
Revised: 22 November 2025
Accepted: 26 November 2025
Published: 28 November 2025

Citation: Akilbekov, A.; Kiryakov, A.; Podshivalov, A.; Ospanova, Z.; Aralbayeva, G.; Popov, A.I.; Baimukhanov, Z.; Junisbekova, D.; Dauletbekova, A. The Role of the Crystal Plane Irradiated by Swift Heavy Ions in the Formation of Defects in $MgAl_2O_4$ Crystals. *Crystals* **2025**, *15*, 1020. https://doi.org/10.3390/cryst15121020

1. Introduction

Magnesium aluminum oxide crystallizes in the spinel phase $MgAl_2O_4$ in equilibrium. Spinel demonstrates very high radiation resistance to high-energy particle irradiation, making it a promising material for optical/diagnostic windows in future thermonuclear reactors. $MgAl_2O_4$ crystals can also be used as materials for various laser media [1], phosphors for solid-state lighting [2], and scintillators [3]. $MgAl_2O_4$ spinel is also used as a substrate for growing thin films [4,5], as an alternative matrix for waste immobilization [6,7], or as a target material in actinide nuclear transmutation [8]. For numerous nuclear applications, extremely high resistance to intense radiation or prolonged exposure to harsh environmental conditions with virtually no swelling is of particular importance [9,10]. This property may be due to the peculiarities of the crystal structure of $MgAl_2O_4$. Oxygen ions form a face-centered cubic structure, Al^{3+} cations with a relatively large ionic radius occupy half of the octahedral gaps, and Mg^{2+} cations with a small radius are in every eighth tetrahedral site [11]. The free volume of the unit cell determines the possibility of forming additional interstitial defects. The cationic sublattice can be disordered under high-energy influences [12]. Spinel crystals have high radiation resistance to fast neutrons due to the

effective recombination of radiation-induced primary Frenkel defects—vacancies and interstitials [13,14]. Cation substitution defects (anti-site defects, or ADs) are also known in spinels. The nature of these defects lies in the localization of aluminum cations Al^{3+} in the position of magnesium Mg^{2+} $Al|^{3+}_{Mg^{2+}}$ and magnesium ions Mg^{2+} in the aluminum position Al^{3+} $Mg|^{2+}_{Al^{3+}}$. The energy of ADs charged (−1 or +1) relative to the regular lattice is significantly lower than for any other elementary lattice defects. This circumstance explains the significant concentration of ADs in synthetic single crystals and optical ceramics, and further irradiation can stimulate the growth of the degree of cation inversion [15–17]. When irradiated with accelerated particle beams, electron and hole color centers (V, F-type, etc.) are created. Such point defects are extremely difficult to detect using structurally oriented methods of studying materials (e.g., XRD or neutronography methods), but even these methods can reveal deviations in fundamental parameters when defect density is high. Methods that are more sensitive to point defects, such as optical absorption or electron paramagnetic resonance (EPR), enable a more accurate assessment of the impact of high-energy beams at low fluences on the formation of elementary structural defects. According to the literature [13,14,18–25], the broad band of complex radiation-induced absorption with peaks at around 4.8 eV and 5.3 eV is mainly due to F^+ and F-centers with an energy of 4.75 eV, while hole color centers (V) are responsible for optical absorption at ~3–4 eV.

One of the most common methods for modeling the interaction of materials with high-energy radiation is irradiation with swift heavy ions (SHI) produced by cyclotron. The interaction of SHI with spinel crystals leads to the creation of latent tracks when electron losses significantly exceed the threshold value of 7.5 keV/nm [26–29]. High-resolution transmission electron microscopy (HRTEM) examination of the surface and cross-section revealed that 670 MeV Bi ions, with an electron energy loss of 36.6 keV/nm, create latent tracks in the surface layer of spinel crystals [30]. It has been established that the ion track remains crystalline, but its structure is disturbed, resulting in the appearance of a visible deformation field.

Our study has established that the arrangement of ions in the crystallographic planes in spinels (100), (110), and (111) have unique features. The ions are arranged in such a way that they form orderly "columns" as well as empty "holes"—areas filled or unfilled with ions along the entire length of the unit cell. Irradiation of single spinel crystals in these specific directions will allow us to study the characteristics of defect formation and establish the role of the crystallographic plane in the interaction of $MgAl_2O_4$ with SHI. In this regard, the aim of this study is to investigate the features of defect formation in $MgAl_2O_4$ crystals with (100), (110), and (111) planes irradiated with 220 MeV Xe ions.

2. Experimental Section

This study used optically transparent $MgAl_2O_4$ spinel crystals (ALINEASON, Frankfurt, Germany) cut in crystallographic planes (100), (110), and (111).

The structure of the $MgAl_2O_4$ crystal lattice is a densely packed anionic oxygen lattice in which two cationic sublattices of aluminum and magnesium are located, occupying the centers of oxygen octahedra and tetrahedra, respectively (Figure 1). The crystal lattice belongs to space group 227 Fd3m. In a typical spinel arrangement, Mg^{2+} ions occupy 1/8 of the tetrahedral positions with T_d symmetry (also known as position A, shown in green in Figure 1). At the same time, Al^{3+} ions occupy 1/2 octahedral positions with D_{3d} symmetry (position B, shown in gray in Figure 1). In partially inverted spinel crystals, trivalent metal ions Al^{3+} can move to tetra positions instead of divalent Mg^{2+} ions. Similarly, Mg^{2+} can move to octa positions instead of Al^{3+}, forming ADs defects with complete charge compensation between each other.

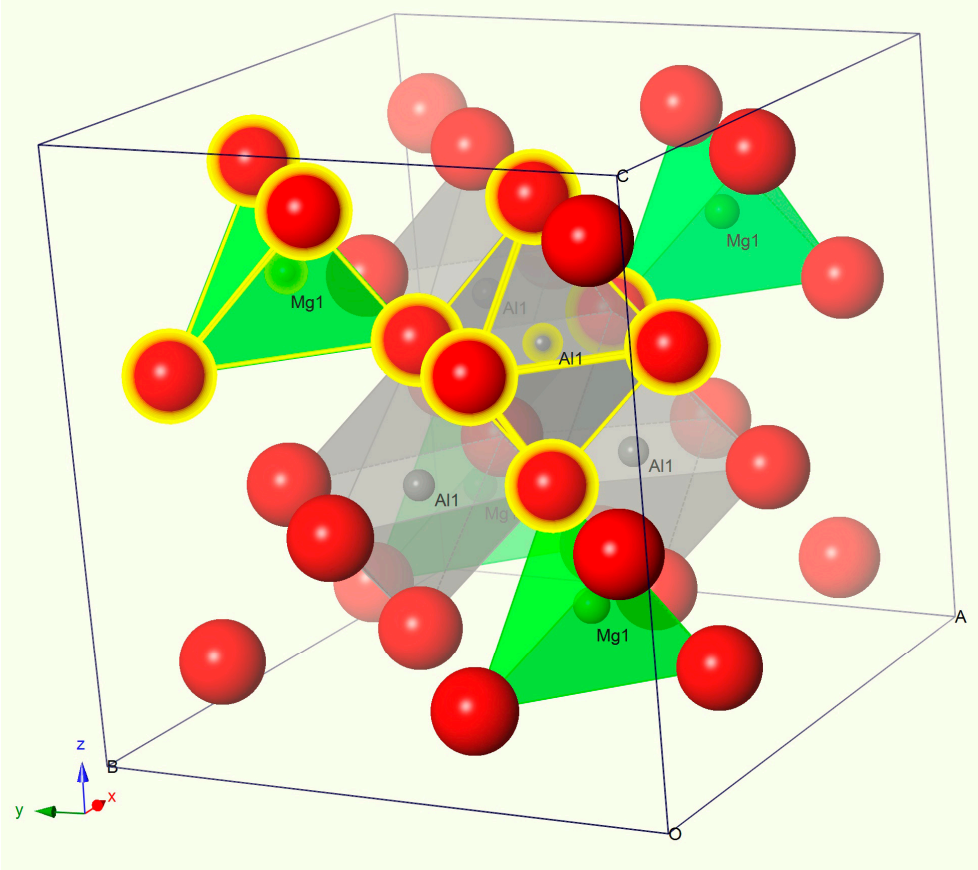

Figure 1. Elementary cubic cell of $MgAl_2O_4$. Color coding scheme used: green—Mg ions; gray—Al ions; red—O ions. Mg and Al positions in tetrahedral and octahedral positions are shown in green and gray, respectively.

The arrangement of ions for different crystallographic planes is shown in Figure 2.

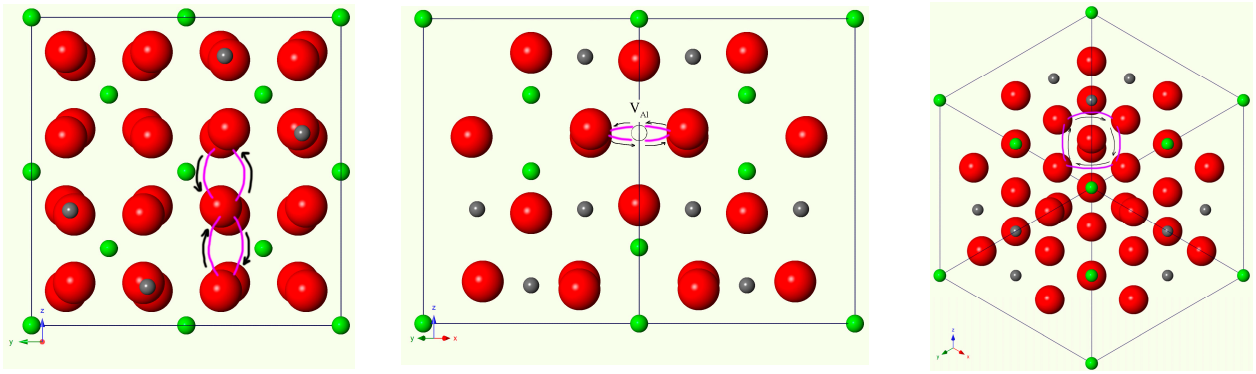

(100) (110) (111)

(**a**) (**b**) (**c**)

Figure 2. Crystallographic planes (100)—(**a**), (110)—(**b**), and (111)—(**c**) for $MgAl_2O_4$ single crystal. Color coding scheme used: green—Mg ions, gray—Al ions, red—O ions, purple lines indicate the equatorial plane of oxygen octahedra.

Analysis of Figure 2 shows that crystals with (110) orientation exhibit a lattice feature in which oxygen anions are arranged in a single row, forming peculiar "columns" (there is no alternation of ions deep inside the crystal along the length of the "column").

The samples under investigation were irradiated with swift heavy ions (SHI) of Xe ions with an energy of 220 MeV at room temperature (RT) perpendicular to the (100), (110), and (111) planes at the DC-60 cyclotron in Astana, Kazakhstan. The fluence range was from 10^{10} to 10^{13} cm^{-2}. The main parameters of Xe ions in $MgAl_2O_4$ crystals were calculated using the SRIM 2013 code [31] and are presented in Table 1 and Figure 3. In addition, Figure 3 shows the distribution of xenon ions in depth. The evenness of the ion beam across the surface of the irradiated sample was checked by scanning the beam in both horizontal and vertical directions, and the variation was no more than 10%. It should be noted that even with such intense irradiation, the crystals retain a high level of transparency (Figure 4).

Table 1. Parameters of 220 MeV Xe ions in $MgAl_2O_4$ single crystals.

Ion and Energy, MeV	Fluence, cm^{-2}	R_p, μm	<S_e>, keV/nm	<Sn>, keV/nm
^{132}Xe, 220	10^{10}–10^{14}	14.12	24.3	0.074

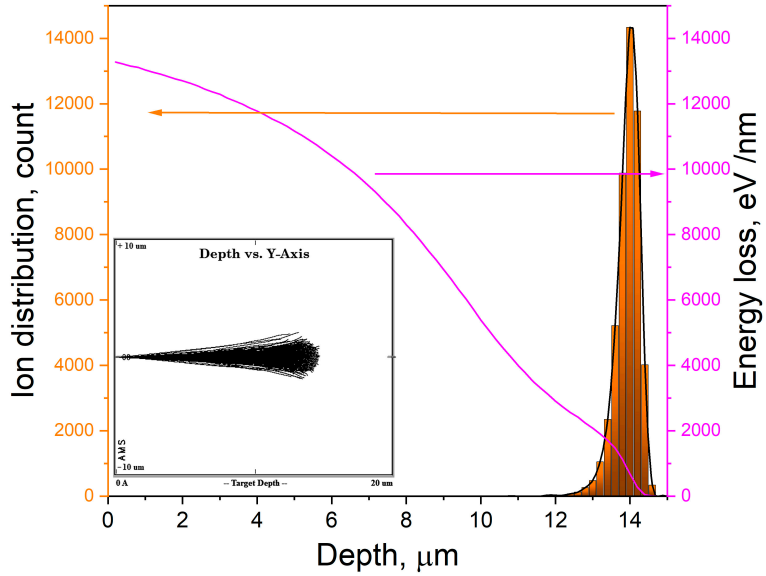

Figure 3. Distribution profile of Xe ions in the near−surface layer of crystals after SHI (orange), as well as the energy loss curve (pink). The inset shows typical deviations in a two-dimensional projection.

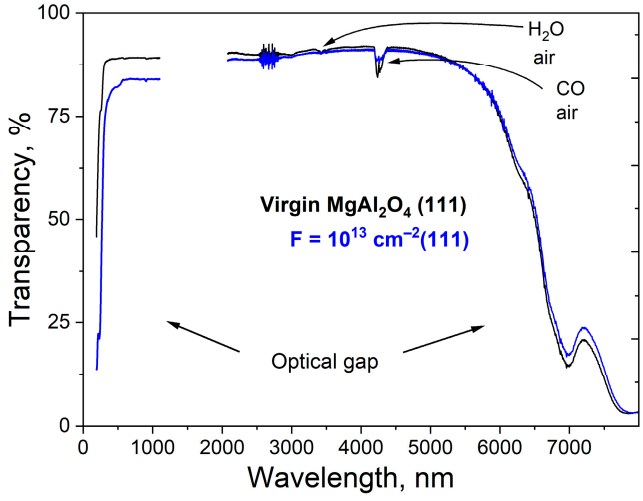

Figure 4. Optical window in a single crystal of magnesium–aluminum spinel (111) before and after irradiation with 220 MeV Xe ions.

The Se/Sn ratio is 328, i.e., specific ionization losses dominate. Nuclear (elastic) energy losses begin to dominate at the end of the ion's path.

Optical spectroscopy in the visible and IR ranges was used in the research. In the range of (190–1100) nm of the virgin and irradiated samples were measured on a Lambda 35 spectrophotometer (PerkinElmer, Waltham, MA, USA). IR spectroscopy was performed on a Shimadzu IR-Prestige-21Fourier spectrophotometer, Kyoto, Japan, (2000–8000) nm. Vacuum ultraviolet (VUV) optical spectroscopy using a Thompson polarizer was recorded using a McPherson VuVAS 1000 PL spectrometer (Chelmsford, MA, USA) with a deuterium light source. The vacuum was maintained at no less than 10^{-3} Pa. Second-order diffraction from the grating monochromator was eliminated using a G-shaped filter with a boundary frequency of 220 nm (transmitting light > 220 nm). Electron paramagnetic resonance spectra (ESR) were recorded using an ELEXSYS 580 spectrometer (Bruker, Karlsruhe, Germany) with resonator frequency set at 9.88 GHz and in the 3250–3800 G range. Standard glass tubes from Bruker were used.

3. Results and Discussions

The interaction of the 220 MeV ^{132}Xe ions (with electron energy losses of 24.3 keV/nm) with the $MgAl_2O_4$ crystal leads to the formation of latent tracks, since the electron losses significantly exceed the threshold value of 7.5 keV/nm [26,27]. The defects formed in this process create optically active centers (color centers) and can be easily detected using optical spectroscopy methods. Based on our analysis of the literature, we have compiled a table of typical optically active centers and their nature; Table 2.

Table 2. Defects in $MgAl_2O_4$ after high-energy irradiation.

Defect	Model	Absorption Band Maximum E_{max}, eV	References
V_c—with captured carriers	$V_1 \rightarrow V_{Al}^{-2} + O^-$ $V_2 \rightarrow V_{Mg}^{-1} + O^-$ $V_{22} \rightarrow V_{Mg\|Al}^{-0} + O^-$	3 − 4	[14,19,21,24]
F^+	V_o + e	4.75	[13,14,18–25]
F	V_o + 2e	5.3	[13,14,18–25]
F_e^{3+} $^6A_{1g} \rightarrow {}^4E_g$	F_e^{3+} in an octahedral position	2.7	[32,33]
F_e^{2+} $^5T_2 \rightarrow {}^5E$	F_e^{2+} in an octahedral position	1.2	[32,33]

V_o—oxygen (anion) vacancy; V_c—cation vacancy.

In spinel crystals, with an increase in fluence, the most significant changes are recorded by VUV spectroscopy in the region of fundamental spinel absorption; Figure 5. As fluency increases, the number of F and F^+ defects in sample (100) also rises, as shown in Figure 5a. This increase is reflected in the absorption spectrum by a higher absorption coefficient in the UV spectral range. In the VUV range, the changes are caused by an increase in static and dynamic disorder, which is reflected in a stronger contribution from the tails of localized zone states. We studied these effects in more detail for $MgAl_2O_4$ single crystals in our work [29]. The optical absorption spectra of sample (110) show small changes in the shape of spectral curves up to a fluence of 10^{13} cm^{-2}. This effect may be due to the (110) crystallographic plane's lower susceptibility to defect accumulation. Once the fluence reaches 10^{13} cm^{-2} and above, track overlap leads to disorder in the crystal structure, which manifests as a shift in the edge of the fundamental absorption and an increase in the concentration of F and F^+ centers [29]. The nature of the change in the optical absorption

coefficient for the sample cut in the (111) plane, shown in Figure 5c, is like that of the (100) sample in Figure 5a. The heterogeneity of the spectral bands near 5.7 eV is due to the mechanical switching of the Γ—shaped filter.

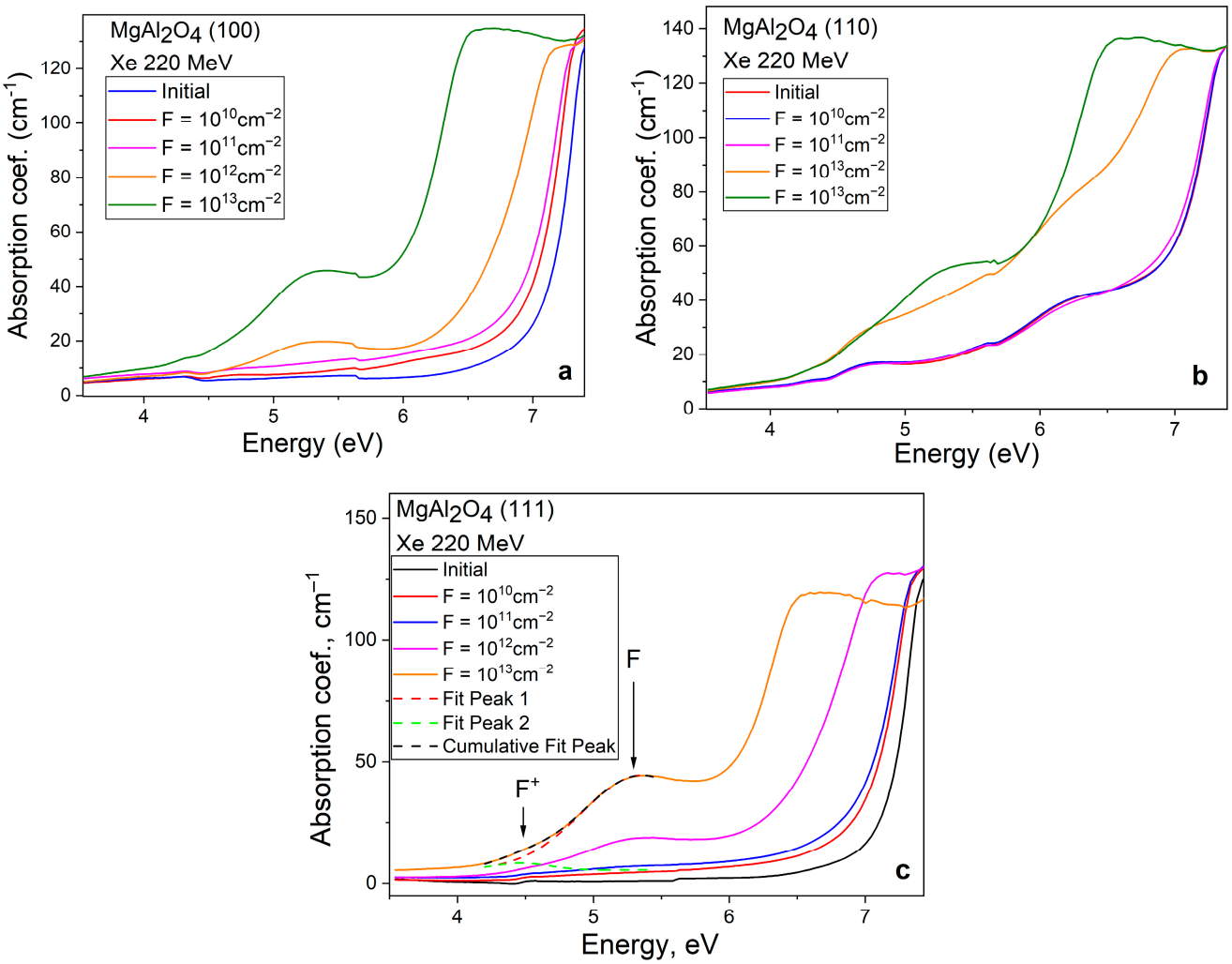

Figure 5. Optical absorption spectra of $MgAl_2O_4$ crystals (100)—(**a**), (110)—(**b**), and (111)—(**c**) before and after SHI irradiation. The 5.7 eV peak in all spectra is associated with the switching of the optical filter. Figure (**c**) shows the deconvolution of the spectrum section into Gaussians.

Analysis of the spectra after irradiation, carried out according to the data in Table 2, shows that the broad absorption band in the range from 4 to 6 eV is a superposition of absorption bands associated with F^+ and F centers of the electron type, while hole centers are responsible for absorption at ~3–4 eV. It should be noted that microimpurities, mainly Fe, Cr, and Mn, also contribute to the absorption spectra (from the IR to the UV spectral region [18–20,34,35]). Of particular interest is the origin of the optical absorption around 6.5 eV, approximately near the edge of the fundamental absorption. According to recent studies of single crystals and $MgAl_2O_4$ optical ceramics using several optical methods [16,29], the E_g value at low temperatures slightly exceeds 8 eV. In the same works, analysis of excitation spectra for various types of emission and phosphorescence led to the conclusion that the spectral range of 6.8–7.4 eV is characteristic of the formation of exciton-like states. This occurs as a result of excitation by photons in the UV range of electron–hole pairs in the tails of localized states, which are drawn into the forbidden zone. ADs defects localize electrons and holes in pairs, causing the formation of bound excitons near charged ADs [16,36]. In the Section 2, Figure 2 shows a characteristic columnar

arrangement of oxygen ions in the crystallographic plane (110). When $MgAl_2O_4$ (110) samples are irradiated by Xe SHI, the generated electronic excitations, such as exciton states, generate bound electron–hole pairs near charged ADs^* during the self-trapping process. In the optical absorption spectra of irradiated crystals (Figure 5), this manifests itself as an increase in the optical absorption band with a maximum of 6.5 eV. It should also be noted that the concentration of such defects (ADs^* + exciton) is higher for sample (110) than for sample (111). It is also essential to consider the fact that some excitons decay into a Frenkel pair of defects when they are self-trapped. Analysis of the number of optically active F centers at a fluence of 10^{13} cm^{-2} shows that in crystals with (110) orientation, 35% more such centers are formed than in crystals with (111) orientation.

The optical absorption spectra shown in Figure 5 demonstrate a set of overlapping spectral lines. The complex nature of optical absorption curves is due to the formation of a set of optically active centers, whose positions, due to their proximity to each other, cannot always be clearly identified. To separate them, both the deconvolution method, considering the Gaussian distribution and known line characteristics [37], and the polarization spectroscopy method were used.

The application of the Gaussian deconvolution method is illustrated in Figure 5c for the optical absorption curve of a sample coated with a fluence of 10^{13} cm^{-2}. It is well known that anionic vacancies (V_O^{2+}) form in $MgAl_2O_4$ crystals after high-energy exposure. Oxygen vacancies are potential traps for negative free charge carriers (electrons). Electrons, when localized at such a vacancy, form an optically active center with its own set of energy levels within the band gap. When a single electron becomes localized, a so-called F^+ center is formed, whereas the localization of two electrons with opposite spins results in the formation of an F center. The positions of the energy level maxima within the band gap for these centers differ by 0.6 eV; however, as a result of spectral line broadening in the absorption spectra, the signals may overlap. The energy transitions between the excited and ground states are well described within the framework of the normal (Gaussian) distribution, according to which there is a 68% probability of finding the desired result within one standard deviation from the mean value, while 99.7% of the probability lies within three standard deviations. Thus, by analyzing the optical absorption curves in the range of 4.2–5.4 eV using Gaussian functions with parameters of half-width and peak positions known from the literature, it is possible to perform a mathematical description of this part of the spectral dependence (shown by the red and green dashed curves in Figure 5c).

Polarized absorption spectra measured using a Thompson polarizer are shown in Figures 6–8 for samples with (100), (110), and (111) orientations, respectively, before and after irradiation. The intensities of the spectral bands associated with the F and F^+ centers in the 4.5–6 eV range remain nearly the same and show no dependence on the polarizer rotation angle. n the VUV range, variations in the optical absorption coefficient under polarized light may be attributed to the formation of exciton-like states at antisite defects in the crystal lattice. The sensitivity of excitons to polarized light is well known from previous studies [36,37].

When the prismatic polarizer is rotated, a broad band of optical absorption in the range of 3–4.5 eV is recorded in the absorption spectrum of crystals (100) and (110). Most likely, V-type centers formed as a result of crystal growth absorb in this area. The angular dependence of the 4.3 eV absorption band in the initial and irradiated (100) and (110) crystals is shown in Figure 8a,b, respectively.

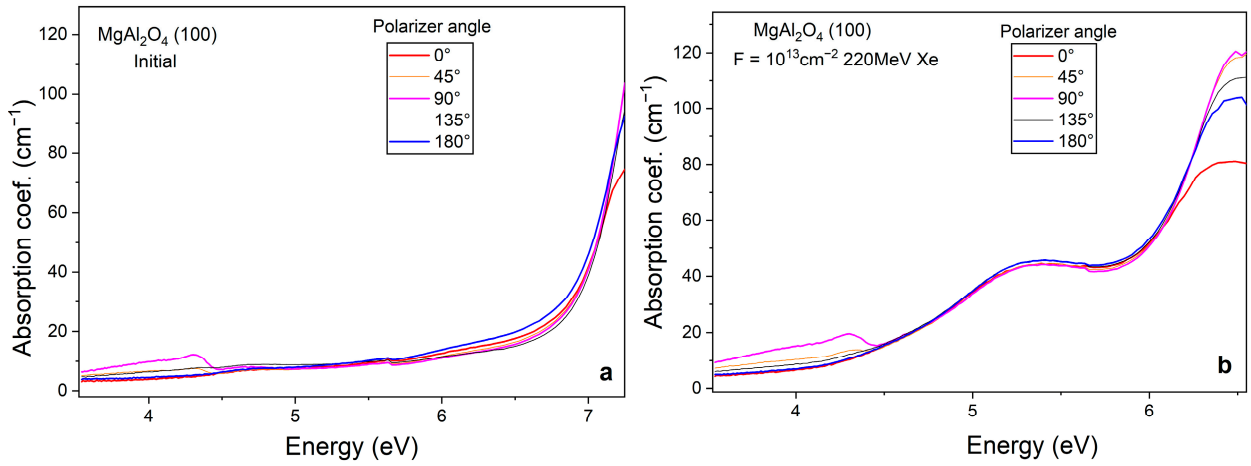

Figure 6. Optical absorption spectra of spinel crystals (100) before (**a**) and after (**b**) ion irradiation with 220 MeV Xe, up to a fluence of 10^{13} cm^{-2}, measured using a Thompson polarizer in an s−polarized beam (s−polarized extraordinary ray).

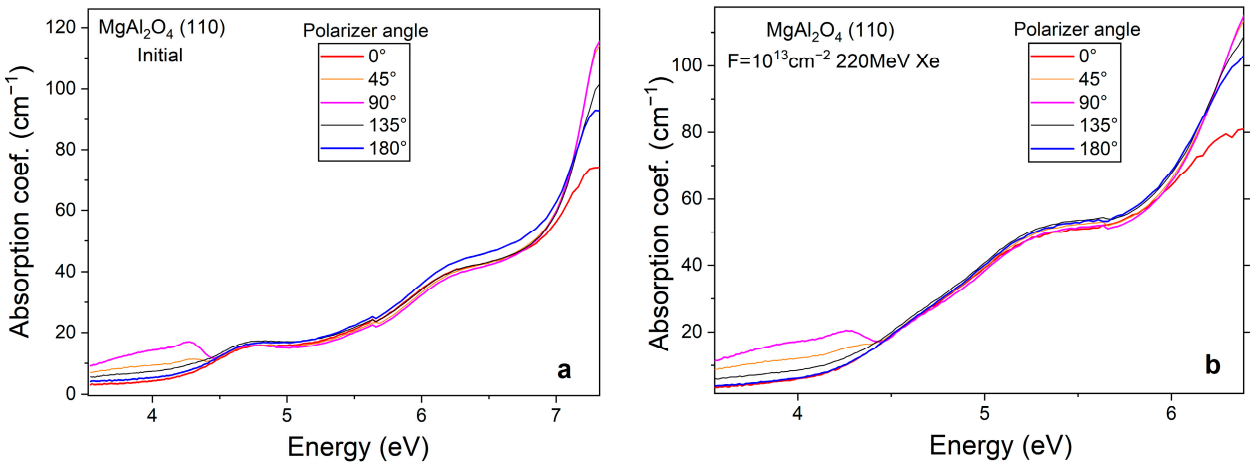

Figure 7. Optical absorption spectra of spinel crystals (110) before (**a**) and after (**b**) ion irradiation with 220 MeV Xe, up to a fluence of 10^{13} cm^{-2}, measured using a Thompson polarizer in an s−polarized beam (s−polarized extraordinary ray).

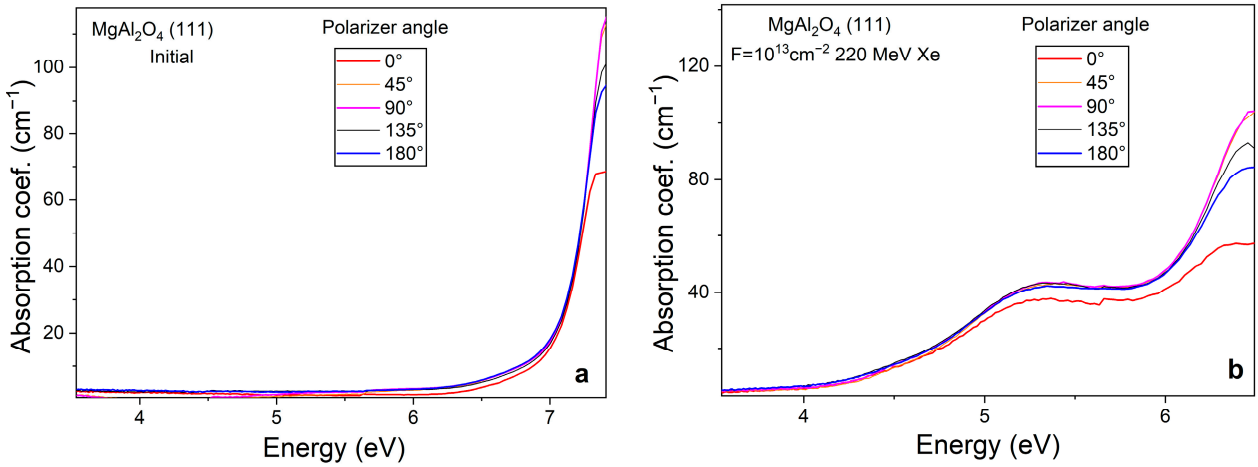

Figure 8. Optical absorption spectra of spinel crystals (111) before (**a**) and after (**b**) ion irradiation with 220 MeV Xe, up to a fluence of 10^{13} cm^{-2}, measured using a Thompson polarizer in an s-polarized beam (s-polarized extraordinary ray).

Figure 9 shows that the signal intensity increases to an angle of 90° and then returns to its initial state at 180°. This behavior is consistent with Malus' law $I = kI_0 \cos^2 \varphi$, where I is the intensity of the transmitted light, I_0 is the intensity of the incident light, k is the transparency coefficient of the prism, and φ is the angle between the polarized light and the sample. In the case of the pattern observed in Figure 9, there is a 90° phase shift caused by the orientation of the sample in the crystal holder relative to the polarized light. The sensitivity of crystals to polarized light is most likely due to the presence of elementary structural defects, which could have arisen during both crystal growth and SHI irradiation. The presence of structural disorder in the initial crystals was previously confirmed by us in [29]. At the same time, under the influence of SHI, new V-type vacancies are also being formed. The creation of such new centers is confirmed by the results of EPR studies; Figure 10.

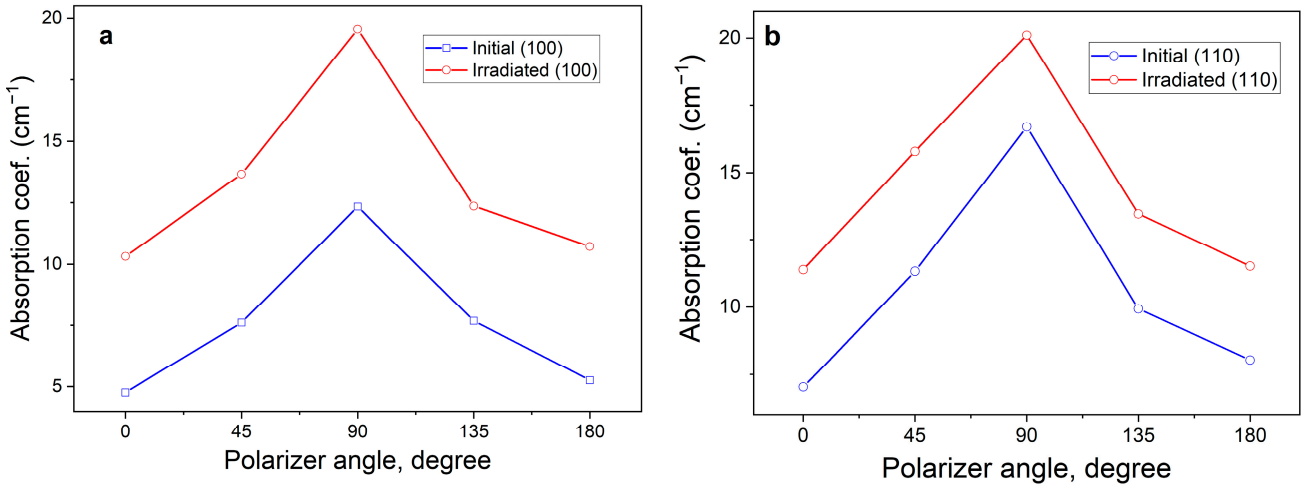

Figure 9. Dependence of the optical absorption coefficient on the angle of rotation of the prismatic polarizer in the 4.3 eV band for (100)—(**a**), (110)—(**b**) planes.

Several signals caused by the formation of cation vacancies with localized (captured) holes (O^-) (V_1 and V_2) centers were recorded in the EPR spectra. The position of the signals detected in this work has a weak angular dependence (in a magnetic field) and azimuthal dependence (change in the crystallographic plane). According to the study conducted in [24], high-energy irradiation of magnesium aluminate spinel crystals can lead to the formation of V_{22} and V_3 type centers. V_{22} centers are complex defects formed by a hole trapped on an oxygen ion and the nearest aluminum site substituted by a magnesium cation $V^{-0}_{Mg|Al} + O^-$ (Table 2). In the investigated samples, the V_{22} and V_3 centers are weakly distinguishable in the EPR spectra, while the main contribution to the EPR signal arises from V_1 and V_2 centers. Signals corresponding to trace amounts of Mn^{2+} ions are also present in the EPR spectra. Such impurities originate from the starting reagents used in the synthesis of both simple oxides (MgO and Al_2O_3) and magnesium aluminate ($MgAl_2O_4$). The Mn^{2+} EPR signal was employed as a reference indicator of the crystal quality. The growth of defect density in both the anion and cation sublattices near the impurity tetrahedrally coordinated Mn^{2+} ion results in the broadening of the hyperfine structure lines observed in the electron paramagnetic resonance spectra. The observed lines in the EPR spectra originate from the interaction between the electron magnetic moment and the nuclear magnetic moment of the Mn^{2+} ion. Consequently, the five lines associated with fine structure caused by spin–orbit coupling are further split into thirty hyperfine lines. However, among the fine-structure transitions, only the central one, $|-1/2, m\rangle \rightarrow |1/2, m\rangle$, exhibits isotropy in the magnetic field [38]. When analyzing the EPR spectra in

the form of the first derivative of the lines, the increase in defect concentration and the decrease in crystallinity are reflected in the growth of the peak-to-peak parameter for each line of the hyperfine splitting signal, as well as in the change in the hyperfine constant A (80.4 Gauss) for Mn^{2+} ions.

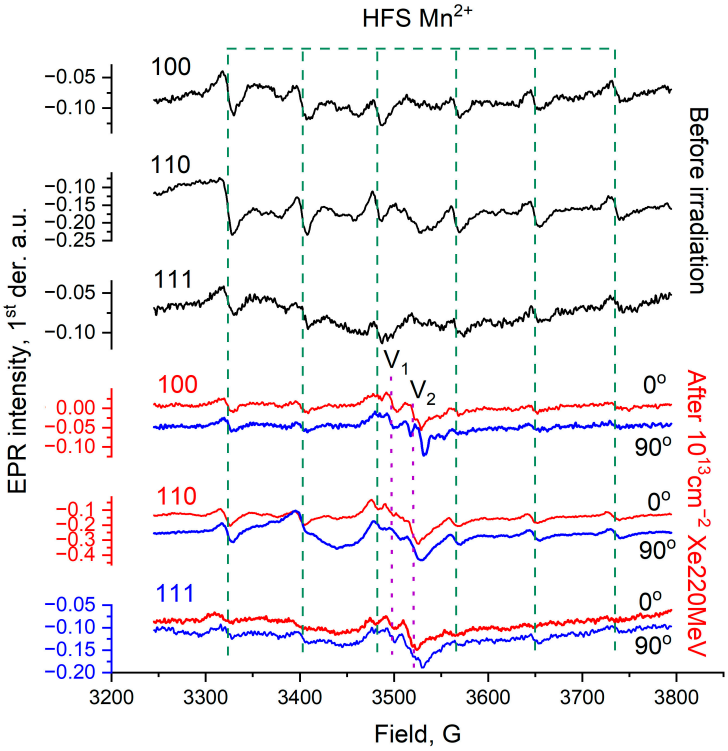

Figure 10. EPR spectra of spinel crystals (100), (110), and (111) before irradiation (black) and after irradiation with the main crystallographic plane oriented in a magnetic field B ∥ (blue) and B⊥ (red). The hyperfine splitting (HFS) of Mn^{2+} acts as a structure-sensitive parameter.

In this case, the hyperfine splitting of manganese ions serves as a marker of the crystallinity of the sample structure, indicating that SHI irradiation does not lead to significant lattice disorder throughout the entire volume (the surface layer itself is severely damaged).

The study conducted in [14] presents the results of computer modeling of the main properties of defective $MgAl_2O_4$ containing one of three V centers. For V_1 center ($V_{Al}^{-2}+O^-$) the ratio Q/e = −0.92, M/μ_B = 0.78, for V_2 ($V_{Mg}^{-1}+O^-$) − Q/e = −0.78, M/μ_B = 0.8, and for V_{22} ($V_{Mg|Al}^{-0}+O^-$) − Q/e = −1.05, M/μ_B = 0.72, where Q and M are the effective atomic charge and magnetic moment of an oxygen ion with a localized (captured) hole (O^-). This allows us to conclude that the formation energy of V_{22} centers is lower than that of other types of centers, and therefore, their concentration should be considerably higher than that of V_1 or V_2 centers. Nevertheless, charge compensation for a magnesium cation substituting an aluminum site [$Mg^{2+}{}_{Al3}{}^{+}$], is mainly achieved through the formation of an aluminum ion occupying a magnesium site [$Al^{3+}{}_{Mg2+}$]. Consequently, this pair of defects constitutes a charge-neutral complex.

The absence of V_{22}-type centers indicates that Mg_{Al} antisite defects mainly localize excitons. During crystal growth, vacancy defects are formed, including V_{Al}-type defects [39]. Such defects act as hole traps. In empty oxygen octahedra, the density of positive charge distribution is localized equatorially. When capturing a hole at such a center, an equatorially distributed charge will interact more effectively with polarized light when the polarization direction coincides, and less effectively when the polarization direction does not coincide with the charge density. For plane (100), the equatorial plane of charge localization is parallel to the electric field stress of the electromagnetic wave. In this case,

there is a single maximum and minimum in the range of the polarizer rotation of 90°. The same applies when the crystallographic plane is (110). For orientation (111), the equatorial plane is located at an angle of 45° to the electric polarization vector. At the same time, the rotation of the polarizer causes the angle between the equatorial plane and the electric polarization vector to remain constant at 45°.

4. Conclusions

Spinel $MgAl_2O_4$ crystals were irradiated with 220 MeV Xe ions in a cyclotron perpendicular to the crystallographic planes (100), (110), and (111). The parameters of Xe ions in $MgAl_2O_4$ crystals have been calculated.

A comprehensive analysis was performed of the optical and paramagnetic centers formed during the interaction of spinel crystals with the (100), (110), and (111) planes and SHI.

Optical absorption spectroscopy analysis shows that SHI irradiation up to a fluence of 10^{13} cm^{-2} results in the most intensive defect formation in crystals cut along the (100) and (111) planes. In contrast, crystals with (110) orientation are more prone to the formation of optically active centers only at higher fluences, above 10^{13} cm^{-2}. Optical absorption spectroscopy using plane-polarized light makes it possible to detect vacancy-type centers $V|_{Al}$ in crystals with (100) and (110) orientations. The behavior of these centers upon rotation of the polarizer follows Malus's law.

Tracks produced by 220 MeV Xe ions do not significantly affect the crystallinity of the studied samples, as evidenced by the unchanged HFS signal of Mn^{2+} in the EPR spectrum. The irradiation with accelerated ions leads to the formation of a number of paramagnetic centers identified as V_1 and V_2. The positions of these centers do not exhibit any considerable shifts upon changing the crystal orientation in the magnetic field.

Author Contributions: Conceptualization, A.A. and A.I.P.; methodology, A.D.; software, G.A.; validation, A.D., A.K., A.P. and Z.B.; formal analysis, A.A.; investigation, A.K., A.P., Z.O. and D.J.; resources, D.J.; data curation, A.D.; writing—original draft preparation, A.D. and A.K.; writing—review and editing, A.K. and A.D.; visualization, D.J.; supervision, A.D.; project administration, G.A.; funding acquisition, A.A. All authors have read and agreed to the published version of the manuscript.

Funding: This research was funded by the Ministry of Science and Higher Education of the Republic of Kazakhstan, grant number AP23488607 «Irradiation temperature effect on damage structure formation in oxides and spinel with swift heavy ions».

Data Availability Statement: The original contributions presented in this study are included in the article. Further inquiries can be directed to the corresponding authors.

Acknowledgments: The work was carried out within the framework of the grant project AP23488607 of the Ministry of Science and Higher Education of the Republic of Kazakhstan. Arseny Kiryakov expresses his gratitude to the Institute of Solid State Chemistry of the Ural Branch of the Russian Academy of Sciences for support (the state assignment No. 124020600024–5). Alma Dauletbekova extends her heartfelt gratitude to the Latvian Academy of Sciences for their continued support.

Conflicts of Interest: The authors declare no conflicts of interest.

References

1. Jouini, A.; Yoshikawa, A.; Brenier, A.; Fukuda, T.; Boulon, G. Optical Properties of Transition Metal Ion-Doped $MgAl_2O_4$ Spinel for Laser Application. *Phys. Status Solidi C Curr. Top. Solid State Phys.* **2007**, *4*, 1380–1383. [CrossRef]
2. Song, E.H.; Zhou, Y.Y.; Wei, Y.; Han, X.X.; Tao, Z.R.; Qiu, R.L.; Xia, Z.G.; Zhang, Q.Y. A Thermally Stable Narrow-Band Green-Emitting Phosphor $MgAl_2O_4$:Mn^{2+} for Wide Color Gamut Backlight Display Application. *J. Mater. Chem. C Mater.* **2019**, *7*, 8192–8198. [CrossRef]

3. Chen, C.F.; Doty, F.P.; Houk, R.J.T.; Loutfy, R.O.; Volz, H.M.; Yang, P. Characterizations of a Hot-Pressed Polycrystalline Spinel: Ce Scintillator. *J. Am. Ceram. Soc.* **2010**, *93*, 2399–2402. [CrossRef]
4. Liu, K.; Zhang, R.; Lu, L.; Mi, S.B.; Liu, M.; Wang, H.; Jia, C.L. Formation of Antiphase Boundaries in CuFe2O4 Films Induced by Rough $MgAl_2O_4$ (001) Substrates. *Thin Solid Film.* **2019**, *680*, 55–59. [CrossRef]
5. Fukami, N.; Wakamatsu, R.; Shinozaki, N.; Wasai, K. Wettability between Porous $MgAl_2O_4$ Substrates and Molten Iron. *Mater. Trans.* **2009**, *50*, 2552–2556. [CrossRef]
6. Weber, W.J.; Ewing, R.C.; Catlow, C.R.A.; Diaz De La Rubia, T.; Hobbs, L.W.; Kinoshita, C.; Matzke, H.; Motta, A.T.; Nastasi, M.; Salje, E.K.H.; et al. Radiation Effects in Crystalline Ceramics for the Immobilization of High-Level Nuclear Waste and Plutonium. *J. Mater. Res.* **1998**, *13*, 1434–1484. [CrossRef]
7. Wang, L.; Liang, T. Ceramics for High Level Radioactive Waste Solidification. *J. Adv. Ceram.* **2012**, *1*, 194–203. [CrossRef]
8. Wiss, T.; Matzke, H. Heavy Ion Induced Damage in $MgAl_2O_4$, an Inert Matrix Candidate for the Transmutation of Minor Actinides. *Radiat. Meas.* **1999**, *31*, 507–514. [CrossRef]
9. Pells, G.P.; Murphy, M.J. The Effects of Transmutation Products on the Radiation-Induced Swelling of Al_2O_3 and $MgAl_2O_4$. *J. Nucl. Mater.* **1991**, *183*, 137–144. [CrossRef]
10. Kinoshita, C.; Zinkle, S.J. Potential and Limitations of Ceramics in Terms of Structural and Electrical Integrity in Fusion Environments. *J. Nucl. Mater.* **1996**, *233–237*, 100–110. [CrossRef]
11. Palik, E.D. Part II. Critics. In *Handbook of Optical Constants of Solids*; Academic Press: San Diego, CA, USA, 1998; p. 789.
12. French, R.H.; Jones, D.J.; Kasowski, R.V.; Ohuchi, F.S.; Bortz, M.L. Temperature Dependence of the Electronic Structure of Oxides: MgO, $MgAl_2O_4$ and Al_2O_3. *Phys. Scr.* **1990**, *41*, 537. [CrossRef]
13. Lushchik, A.; Feldbach, E.; Kotomin, E.A.; Kudryavtseva, I.; Kuzovkov, V.N.; Popov, A.I.; Seeman, V.; Shablonin, E. Distinctive Features of Diffusion-Controlled Radiation Defect Recombination in Stoichiometric Magnesium Aluminate Spinel Single Crystals and Transparent Polycrystalline Ceramics. *Sci. Rep.* **2020**, *10*, 7810. [CrossRef]
14. Tatarchuk, T. Studying the Defects in Spinel Compounds: Discovery, Formation Mechanisms, Classification, and Influence on Catalytic Properties. *Nanomaterials* **2024**, *14*, 1640. [CrossRef]
15. Gilbert, C.A.; Smith, R.; Kenny, S.D.; Murphy, S.T.; Grimes, R.W.; Ball, J.A. A Theoretical Study of Intrinsic Point Defects and Defect Clusters in Magnesium Aluminate Spinel. *J. Phys. Condens. Matter* **2009**, *21*, 275406. [CrossRef]
16. Feldbach, E.; Kudryavtseva, I.; Mizohata, K.; Prieditis, G.; Räisänen, J.; Shablonin, E.; Lushchik, A. Optical Characteristics of Virgin and Proton-Irradiated Ceramics of Magnesium Aluminate Spinel. *Opt. Mater.* **2019**, *96*, 109308. [CrossRef]
17. Sickafus, K.F.; Larson, A.C.; Nastasi, N.; Yu, M.; Hollenberg, G.W.; Garner, F.A.; Bradt, R.C. Cation disorder in high dose, neutron-irradiated spinel. *J. Nucl. Mater.* **1995**, *219*, 128–134. [CrossRef]
18. Summers, G.P.; White, G.S.; Lee, K.H.; Crawford, J.H. Radiation Damage in $MgAl_2O_4$. *Phys. Rev. B* **1980**, *21*, 2578–2584. [CrossRef]
19. White, G.S.; Jones, R.V.; Crawford, J.H. Optical Spectra of $MgAl_2O_4$ Crystals Exposed to Ionizing Radiation. *J. Appl. Phys.* **1982**, *53*, 265–270. [CrossRef]
20. Cain, L.S.; Pogatshnik, G.J.; Chen, Y. Optical Transitions in Neutron-Irradiated $MgAl_2O_4$ Spinel Crystals. *Phys. Rev. B* **1988**, *37*, 2645–2652. [CrossRef]
21. Gritsyna, V.T.; Afanasyev-Charkin, I.V.; Kazarinov, Y.G.; Sickafus, K.E. Optical Transitions in Magnesium Aluminate Spinel Crystals of Different Compositions Exposed to Irradiation. *Nucl. Instrum. Methods Phys. Res. B* **2004**, *218*, 264–270. [CrossRef]
22. Costantini, J.M.; Lelong, G.; Guillaumet, M.; Weber, W.J.; Takaki, S.; Yasuda, K. Color-Center Production and Recovery in Electron-Irradiated Magnesium Aluminate Spinel and Ceria. *J. Phys. Condens. Matter* **2016**, *28*, 325901. [CrossRef]
23. Ibarra, A.; López, F.J.; Jiménez De Castro, M. V Centers in $MgAl_2O_4$ Spinels. *Phys. Rev. B* **1991**, *44*, 7256–7262. [CrossRef] [PubMed]
24. Lushchik, A.; Dolgov, S.; Feldbach, E.; Pareja, R.; Popov, A.I.; Shablonin, E.; Seeman, V. Creation and Thermal Annealing of Structural Defects in Neutron-Irradiated $MgAl_2O_4$ Single Crystals. *Nucl. Instrum. Methods Phys. Res. B* **2018**, *435*, 31–37. [CrossRef]
25. Seeman, V.; Feldbach, E.; Kärner, T.; Maaroos, A.; Mironova-Ulmane, N.; Popov, A.I.; Shablonin, E.; Vasil'chenko, E.; Lushchik, A. Fast-Neutron-Induced and as-Grown Structural Defects in Magnesium Aluminate Spinel Crystals with Different Stoichiometry. *Opt. Mater.* **2019**, *91*, 42–49. [CrossRef]
26. Zinkle, S.J.; Matzke, H.; Skuratov, V.A. Microstructure of Swift Heavyion Irradiated $MgAl_2O_4$ Spinel. *MRS Online Proc. Libr. (OPL)* **1998**, *540*, 299. [CrossRef]
27. Zinkle, S.J.; Skuratov, V.A. Track Formation and Dislocation Loop Interaction in Spinel Irradiated with Swift Heavy Ions. *Nucl. Instrum. Methods Phys. Res. B* **1998**, *141*, 737–746. [CrossRef]
28. Akilbekov, A.; Kiryakov, A.; Baubekova, G.; Aralbayeva, G.; Dauletbekova, A.; Akylbekova, A.; Ospanova, Z.; Popov, A.I. Optical Characteristics of $MgAl_2O_4$ Single Crystals Irradiated by 220 MeV Xe Ions. *Materials* **2023**, *16*, 6414. [CrossRef]
29. Akilbekov, A.; Kiryakov, A.; Dauletbekova, A.; Aralbayeva, G.; Akylbekova, A.; Ospanova, Z. Unveiling the Structural and Optical Properties of $MgAl_2O_4$ Single Crystals Irradiated by Swift Heavy Ions. *Materials* **2024**, *17*, 344. [CrossRef]

30. Skuratov, V.; Korolik, O.; Mamatova, M.; O'Connell, J.; Kirilkin, N.; Dauletbekova, A.; Akilbekov, A. Photoluminescence and Structural Characterization of $MgAl_2O_4$ Irradiated with Swift Bi Ions. *J. Lumin.* **2025**, *283*, 121259. [CrossRef]
31. Ziegler, J.F.; Ziegler, M.D.; Biersack, J.P. SRIM—The Stopping and Range of Ions in Matter (2010). *Nucl. Instrum. Methods Phys. Res. B* **2010**, *268*, 1818–1823. [CrossRef]
32. Rossman, G.R.; Taran, M.N. Spectroscopic Standards for Four- and Fivefold-Coordinated Fe^{2+} in Oxygen-Based Minerals. *Am. Miner.* **2001**, *86*, 896–903. [CrossRef]
33. Taran, M.N.; Koch-Muller, M.; Langer, K. Electronic absorption spectroscopy of natural (Fe^{2+}, F^{3+})-bearing spinels of spinel s.s.-hercynite and gahnite-hercynite solid solutions at different temperatures and high-pressure. *Phys. Chem. Miner.* **2005**, *32*, 175–188. [CrossRef]
34. Borges, P.D.; Cott, J.; Pinto, F.G.; Tronto, J.; Scolfaro, L. Native Defects as Sources of Optical Transitions in $MgAl_2O_4$ Spinel. *Mater. Res. Express* **2016**, *3*, 076202. [CrossRef]
35. Mironova-Ulmane, N.; Skvortsova, V.; Pavlenko, A.; Feldbach, E.; Lushchik, A.; Lushchik, C.; Churmanov, V.; Ivanov, D.; Ivanov, V.; Aleksanyan, E. Luminescence and EPR Spectroscopy of Neutron-Irradiated Single Crystals of Magnesium Aluminium Spinel. *Radiat. Meas.* **2016**, *90*, 122–126. [CrossRef]
36. Boldyrev, K.N.; Mostovshchikova, E.V.; Titov, A.N. Infrared Transmission Spectra of TiS_3: Fundamental Absorption Edge, Phonons, and Excitons. *JETP Lett.* **2024**, *120*, 565–572. [CrossRef]
37. Gannan, K.J.; Drescher, L.B.; Quintero-Bermudez, R.; Rana, N.; Huang, C.; Schafer, K.; Gaarde, M.B.; Leone, S.R. Polarization-resolved core exciton dynamics in LiF using attosecond transient absorption spectroscopy. *Phys. Rev. B* **2025**, *111*, 134306. [CrossRef]
38. Singh, V.; Chakradhar, R.P.S.; Rao, J.L.; Kim, D.-K. Synthesis, characterization, photoluminescence and EPR investigations of Mn doped $MgAl_2O_4$ phosphors. *J. Solid State Chem.* **2007**, *180*, 2067–2074. [CrossRef]
39. Sawai, S.; Uchino, T. Visible Photoluminescence from $MgAl_2O_4$ Spinel with Cation Disorder and Oxygen Vacancy. *J. Appl. Phys.* **2012**, *112*, 103523. [CrossRef]